A SSVEP-Based Brain–Computer Interface With Low-Pixel Density of Stimuli

Jiayuan Meng, Hui Liu, Qiaoyi Wu, Hongzhan Zhou, Wenqiang Shi, Lin Meng, *Member, IEEE*, Minpeng Xu, *Senior Member, IEEE*, and Dong Ming, *Senior Member, IEEE*

***Abstract*— The brain-computer interface (BCI) based on the steady-state visual evoked potential (SSVEP) has drawn widespread attention due to its high communication speed and low individual variability. However, there is still a need to enhance the comfort of SSVEP-BCI, especially considering the assurance of its effectiveness. This study aims to achieve a perfect balance between comfort and effectiveness by reducing the pixel density of SSVEP stimuli. Three experiments were conducted to determine the most suitable presentation form (flickering square vs. flickering checkerboard), pixel distribution pattern (random vs. uniform), and pixel density value (100%, 90%, 80%, 70%, 60%, 40%, 20%). Subjects' electroencephalogram (EEG) and fatigue scores were recorded, while comfort and effectiveness were measured by fatigue score and classification accuracy, respectively. The results showed that the flickering square with random pixel distribution achieved a lower fatigue score and higher accuracy. EEG responses induced by stimuli with a square-random presentation mode were then compared across various pixel densities. In both offline and online tests, the fatigue score decreased as the pixel density decreased. Strikingly, when the pixel density was above 60%, the accuracies of low-pixel-density SSVEP were all satisfactory (>90%) and showed no significant difference with that of the conventional 100%-pixel density. These results support the feasibility of using 60%-pixel density with a square-random presentation mode to improve the comfort of SSVEP-BCI, thereby promoting its practical applications in communication and control.**

Manuscript received 25 July 2023; revised 27 September 2023; accepted 23 October 2023. Date of publication 31 October 2023; date of current version 14 November 2023. This work was supported in part by the National Key Research and Development Program of China under Grant 2022YFF1202500; in part by the National Natural Science Foundation of China under Grant 81925020, Grant 62106173, Grant 62122059, and Grant 61976152; in part by the General Projects of Postdoctoral Science Foundation of China under Grant 2022M712364; and in part by the Tianjin Natural Science Foundation under Grant 22JCYBJC01480. *(Corresponding authors: Minpeng Xu; Dong Ming.)*

This work involved human subjects or animals in its research. Approval of all ethical and experimental procedures and protocols was granted by the Institutional Review Board at Tianjin University under Application No. TJUE-2021-055.

Jiayuan Meng, Lin Meng, Minpeng Xu, and Dong Ming are with the Academy of Medical Engineering and Translational Medicine, Tianjin University, Tianjin 300072, China, and also with the Haihe Laboratory of Brain–Computer Interaction and Human–Machine Integration, Tianjin 300392, China (e-mail: minpeng.xu@tju.edu.cn; richardming@tju.edu.cn).

Hui Liu, Qiaoyi Wu, Hongzhan Zhou, and Wenqiang Shi are with the Academy of Medical Engineering and Translational Medicine, Tianjin University, Tianjin 300072, China.

This article has supplementary downloadable material available at https://doi.org/10.1109/TNSRE.2023.3328917, provided by the authors.

Digital Object Identifier 10.1109/TNSRE.2023.3328917

***Index Terms*— Brain–computer interface, steady-state visual evoked potential, low-pixel density, comfort, classification accuracy.**

I. Introduction

THE brain-computer interface (BCI) provides a direct communication pathway between the central nervous system and external devices [1], [2]. It encompasses both invasive and noninvasive measures. Among the noninvasive BCIs, the one based on steady-state visual evoked potential (SSVEP) has drawn widespread attention owing to its high communication speed, minimal training required, and low individual variability [3], [4], [5]. In SSVEP-BCI, two critical aspects are the encoding and decoding methods, which correspond to the paradigm and algorithms, respectively. Past decades have witnessed unprecedented progress of SSVEP decoding: the information transfer rate (ITR) has increased by approximately three times since the introduction of canonical correlation analysis (CCA) with individual calibration data and task-related component analysis (TRCA). Moreover, the accuracy has increased by close to 10% with the introduction of filter-bank technology [6], [7], [8], [9]. However, despite significant progress in decoding, there have been few studies exploring how to achieve the perfect balance between effectiveness and comfort in SSVEP-BCI from the encoding perspective. This limitation hampers its further development and potential improvements.

Current encoding studies on SSVEP-BCI have primarily focused on improving effectiveness (decoding accuracy) by adjusting stimuli to trigger larger electroencephalogram (EEG) responses, and enhancing comfort by using high-frequency (>30 Hz) flicker stimulation. Common stimulus-adjusting methods include magnifying stimuli size [10], [11], [12], enhancing luminance contrast [13], [14], [15], and changing the color [16], [17]. What they have in common is the significant enhancement of stimulus intensity perceived by the subjects. However, increasing stimulus intensity can lead to significant fatigue reported by subjects, making it challenging to use the system for extended periods. The lack of comfort has become a major challenge for SSVEP-BCI [18], [19], [20]. A recently widespread studied solution is the adoption of high-frequency SSVEP (>30 Hz, HF-SSVEP). Except for replacing the traditional low-frequency flickers with high-frequency ones, recent studies further developed time-frequency, frequency-phase, space-frequency, and time-space-frequency strategies to optimize both comfort and

effectiveness of HF-SSVEP [21], [22], [23], [24]. However, high-frequency SSVEP, especially above 40 Hz, still faces challenges as the responses may not be robust and could be too small to decode. Therefore, it is of vital importance to a develop new encoding strategy that can achieve a better balance between comfort and effectiveness of SSVEP.

Reducing the pixel density of stimuli appears to be a promising method for achieving a perfect balance between comfort and effectiveness of SSVEP-BCI. By decreasing the number of luminous pixels, the stimulus intensity is reduced, which can alleviate subjects' fatigue. Interestingly, this reduction in pixel density may not affect the strength of neural responses induced by SSVEP, meaning effectiveness may remain constant even as pixel density decreases. The proposal for this approach is based on the center-periphery antagonism effect of retina [25], [26], [27]. Bipolar and ganglion cells in the second and third layers of the retina have center-periphery antagonism receptive fields, which react oppositely to stimuli located at the center and periphery of the receptive field. A macroscopical manifestation of this effect is that the boundaries between light and dark tend to induce larger responses [28], [29]. Consequently, reducing pixel density creates more discrete areas with increased boundaries, potentially triggering larger neural responses. This boundary-related enhancement is expected to counter the decrease caused by intensity reduction.

Although this proposal seems theoretically reasonable, there is a lack of studies investigating the feasibility of low-pixel-density stimuli in optimizing SSVEP-BCI, and many critical parameters remain unknown. There are at least three problems that need investigating about the low-pixel-density SSVEP. Firstly, it remains unclear whether the response enhancement induced by the center-periphery antagonism effect makes sense in the SSVEP paradigm. Additionally, the proper range of pixel density that can satisfy both comfort and effectiveness need further investigation. Secondly, it is uncertain whether the common stimulus presentation form (flickering square vs. flickering checkerboard) and pixel distribution pattern (random vs. uniform) have an impact on low-pixel-density SSVEP. Thirdly, the effectiveness of low-pixel-density SSVEP in an online test requires evaluation. To address these questions, this study conducted three experiments. In the first experiment, we found that flickering square with a random pixel distribution (i.e., square-random) was a more suitable presentation mode for low-pixel-density SSVEP. The second experiment confirmed that a pixel density range of 60% to 90% was suitable. Finally, the third experiment compared the online performance induced by 100%-, 80%-, 60%-, 40%- and 20%-pixel-density SSVEP stimuli, and showed that the 60%-pixel-density condition achieved an online accuracy of 90.10±8.44%, which was almost the same as that of 100%. Moreover, it demonstrated much better comfort than 100%. These findings present a new encoding strategy for effectively balancing the comfort and effectiveness of SSVEP-BCI.

II. Materials and Methods

A. Participants

This study included three experiments, each involving different numbers of subjects: 14, 20, and 12 participants, aged between 18 and 23 years, and all right-handed. Among them, 5 females, 8 females, and 6 females participated in experiment 1, 2 and 3, respectively. All participants had normal or corrected-to-normal vision, were free from psychological or neurological disorders, and had sufficient rest before the experiments. Experimental procedures involving human subjects were approved by the Institutional Review Board at Tianjin University. All possible consequences of the experiment were explained, and written informed consent was obtained from each subject.

B. Design of the Experimental Paradigm

Experiment 1 aimed to investigate three factors related to low-pixel-density SSVEP stimuli, including two presentation forms (flickering square vs. flickering checkerboard), two distribution patterns (random vs. uniform), and five levels of pixel density (100%, 80%, 60%, 40%, 20%). As Fig. 1(a) shows, the screen was divided into 2 × 4 parts, with a flickering square (left) or flickering checkerboard (right) located in each part, and each target occupying 180 × 180 pixels. The two chosen presentation forms are commonly used in SSVEP-BCI. Fig. 1(b) shows examples of stimuli with different pixel densities, distribution patterns, and presentation forms. The 100%-pixel-density stimulus and background were set to white and black, corresponding to the RBG value of (255, 255, 255) and (0, 0, 0), respectively. Here, pixel density was defined as the ratio of flickering pixels (i.e., white pixels) to the total pixels in the stimulus. The lower the pixel density, the weaker the stimulus would be. Moreover, it is believed that visual perception is affected by the distribution pattern of pixels. Thus, this study compared EEG responses induced by two typical distribution patterns: random and uniform. In the uniform pattern, the flickering pixels were regularly arranged, maintaining consistent pixel density throughout the stimulus. On the other hand, in the random pattern, the flickering pixels were randomly assigned to different locations and remained consistent in a single trial, which was kept changed across trials as well as subjects. But the length difference of light-dark boundaries brought about by this change were statistically controllable. The experiment employed eight frequencies, i.e., 8Hz, 9Hz, 10Hz, 11Hz, 12Hz, 13Hz, 14Hz, 15Hz. The stimulus interface was displayed on a 24-inch monitor with a screen resolution (pixels) of 1920×1080 and a refresh rate of 240 Hz.

Fig.2 illustrates experiment procedures. A target instruction was cued by a green border before each stimulus lasting 1000ms. EEG responses induced by distinct pixel-density stimuli were compared in four stimulus-presenting modes: square-uniform, square-random, checkerboard-uniform and checkerboard-random (4 modes × 5 pixel densities = 20 types in total). The modes of stimuli and their frequencies were conducted randomly. Each condition (20 types × 8 frequencies) consisted of five trials. In the subsequent classification, four trials were used for training and five-fold cross-validation was performed.

Based on experiment 1, experiment 2 only included the square flicker with random distribution. Pixel densities of 100%, 90%, 80%, 70%, 60%, 40% and 20% were selected. The intervals of pixel density higher than 60% were reduced,

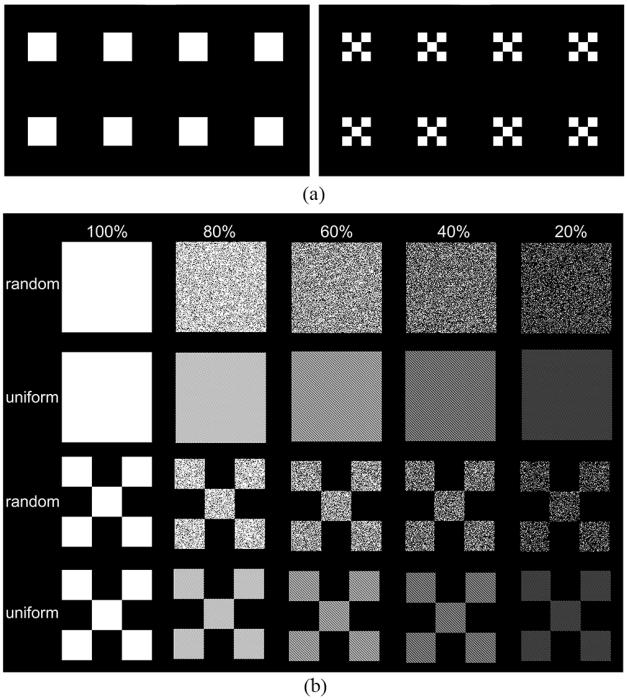

Fig. 1. Stimulus parameter settings. (a) Two presentation forms (square flicker vs. checkerboard flip). (b) Two distribution patterns (random vs. uniform), five levels of pixel density (100%, 80%, 60%, 40%, 20%).

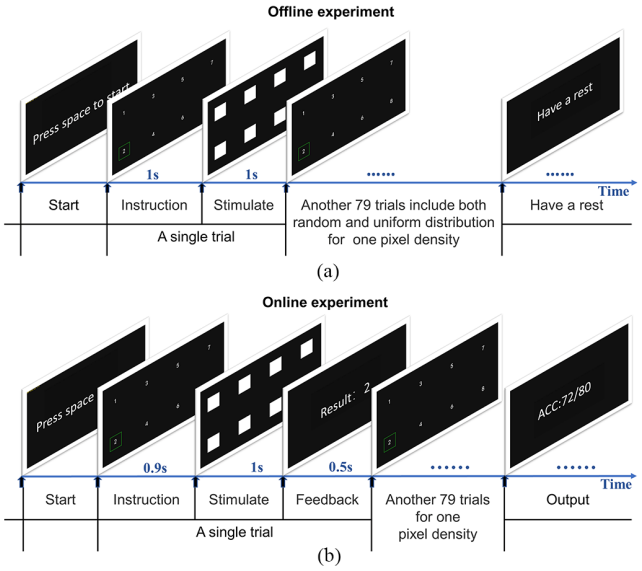

Fig. 2. Experiment procedures. (a) Procedures of experiment 2 (1 block): an offline test for finding a proper pixel-density range. (b) Procedures of experiment 3 (1 block): an online test comparing 100%-, 60%-, 40%- and 20%-pixel density.

aiming to find a more detailed and appropriate range of pixel density. Moreover, due to that SSVEP performance decreased significantly when the pixel density was below 60%, no further attention was given to that range. Each condition was tested in ten trials. In the subsequent classification, nine trials were used for training and ten-fold cross-validation was performed. The procedures of a block in experimen2 are showed in Fig. 2(a).

Experiment 3 involved an online test to investigate the effect of the low-pixel-density encoding strategy. The performances related to 100%-, 80%-, 60%-, 40%-, 20%-pixel density stimuli were compared in square flicker with random distribution. Four periods were included in the online test: model construction, visual stimulation, data processing, and instruction feedback. Specifically, subjects were first asked to conduct an offline SSVEP test. The procedure for the offline test was consistent with Experiment 2. 10 trials were obtained for each condition to establish the corresponding template. The online SSVEP experiment then commenced, during which eight target frequencies randomly appeared. Detailed procedures are shown in Fig. 2(b). Classification results were displayed on the screen and lasted for 500 ms. There were 10 trials for each frequency at each pixel density.

C. Subjective Fatigue Rating

Comfort was measured using a fatigue score, which participants provided at the end of each experiment. A ten-point scale was used to quantify the subjective level of fatigue experienced. Subjects were asked to rate each pixel density according to their subjective feelings. The score had to be an integer between 1 and 10. In particular, 1 indicated the lowest perceived fatigue, and 10 indicated the highest. Consequently, a higher score represented a greater sense of fatigue (i.e., less comfort). Finally, the subjective scores of all subjects were averaged under each pixel density for comparison.

D. EEG Recording and Pre-Processing

EEG signals from 64 electrodes were recorded by a NeuroScan Synamps2 system at a sample rate of 1000 Hz, with the impedance of each electrode being less than 10 KΩ. The electrodes were positioned on the scalp according to the International 10-20 system, with the prefrontal lobe and the top of head serving as ground and reference, respectively.

Considering the latency of the visual nervous system conduction signal following the stimulus presentation, the data were extracted from 140 ms post-stimulus onset, and a total of 1000 ms of data were extracted for further analyses. The data were then filtered using infinite impulse response (IIR) bandpass filters with cutoff frequencies of 5 Hz and 90 Hz, and a notch filter at 50 Hz.

E. Classification Algorithm

The task-related component analysis (TRCA) and its ensembled version (eTRCA), along with the filter-bank technology, were used for classification. All results were calculated after leave-one-out cross-validation.

1) **TRCA**

TRCA is a classical algorithm for decoding SSVEP signals that was first proposed by Tanaka et al. [30], [31] for extracting task-related components (TRCs) in functional near-infrared imaging (fNIRS) data. In 2018, Nakanishi et al. [6] found TRCA effectively improved the signal-to-noise ratio and suppressed spontaneous EEG activities by maximizing repeatability between multiple trials in SSVEP. Different from the conventional SSVEP decoding algorithm, the signal template of TRCA is not restricted to artificially constructed models with

sinusoidal waveforms. Instead, TRCs consider individual variability information, making it theoretically applicable for decoding any characteristic signal with a stable waveform or time-phase-locked characteristics.

Let N_e, N_t, N_c, N_p denote the number of stimulus frequencies, trials, channels, and sampling points, respectively. For EEG dataset $\boldsymbol{\chi} \in \mathbb{R}^{N_e \times N_t \times N_c \times N_p}$ preprocessed with band-pass filtering (i.e. zero-mean normalization), the i th trial data of k th stimulus is denoted as $\mathbf{X}_k^i \in \mathbb{R}^{N_c \times N_p}$. The one-dimensional spatial filter $\hat{\omega}_k \in \mathbb{R}^{1 \times N_c}$ can be calculated using the following equation:

$$\begin{aligned}\widehat{\boldsymbol{\omega}}_k &= \underset{\omega_k}{\operatorname{argmax}} \frac{\sum_{j=1, j \pm i}^{N_t} \sum_{i=1}^{N_t} \operatorname{Cov}\left(\omega_k \boldsymbol{X}_k^i \boldsymbol{\omega}_k \boldsymbol{X}_k^j\right)}{\sum_{i=1}^{N_t} \operatorname{Var}\left(\boldsymbol{\omega}_k \boldsymbol{X}_k^i\right)} \\ &= \underset{\omega_k}{\operatorname{argmax}} \frac{\omega_k s_k \omega_k^T}{\omega_k \boldsymbol{Q}_k \omega_k{}^T} \end{aligned} \tag{1}$$

where,

$$Q_k = \frac{1}{N_t - 1} \sum_{i=1}^{N_t} X_k^i X_k^{i\,T} \tag{2}$$

$$\begin{aligned} S_k &= \frac{1}{N_t - 1} \sum_{j=1, j \neq i}^{N_t} \sum_{i=1}^{N_t} X_k^i X_k^j \\ &= \frac{1}{N_t - 1} \bar{X}_k \bar{X}_k{}^T - Q_k, \end{aligned}$$

$$\bar{X}_k = \frac{1}{N_t} \sum_{i=1}^{N_t} X_k^i \tag{3}$$

Since $\bar{X}_k$ can represent the pure evoked feature signal to some extent when training samples are relatively sufficient, the objective function (2) can be rewritten as:

$$\begin{aligned}\widehat{\boldsymbol{\omega}}_k &= \underset{\omega_k}{\operatorname{argmax}} \frac{\omega_k \left(\bar{x}_k \bar{x}_k^T\right) \omega_k^T}{\omega_k Q_k \omega_k^T} - 1 \\ &= \underset{\omega_k}{\operatorname{argmax}} \frac{\omega_k \left(\bar{x}_k \bar{X}_k^T\right) \omega_k^T}{\omega_k \left(\sum_{i=1}^{N_t} \boldsymbol{X}_k^i \boldsymbol{X}_k^{i\,T}\right) \omega_k^T} \end{aligned} \tag{4}$$

The equation (4) shows that the objective function of TRCA aims to find a projection vector that maximizes the ratio of feature signal energy to the original signal energy, while preserving the time-frequency characteristics of the signal itself, which is the theoretical basis for the excellent performance of TRCA. The spatial filtering is applied to the single-trial test signal $\mathbf{Y} \in \mathbb{R}^{N_c \times N_p}$ and the category is determined by the Pearson correlation coefficient.

$$\rho_k = \operatorname{corr}\left(\boldsymbol{\omega}_k \overline{\boldsymbol{X}}_k, \boldsymbol{\omega}_k \boldsymbol{Y}\right) \tag{5}$$

$$\hat{k} = \max_k \{\rho_k \mid k = 1, 2, \ldots, N_e\} \tag{6}$$

2) **Filter-Bank Technology**

The filter bank (FB) technique enhances the classification performance of SSVEP-based BCIs by exploiting the fundamental frequency and higher harmonics of SSVEP signals in different filter passbands. Chen et al. [7] first proposed to apply the FB technique to the CCA algorithm and optimized the sub-band design and the weighting scheme of the sub-band features. The FB technique integrates band-specific classification features to effectively utilize SSVEP EEG information, and many studies have demonstrated its effectiveness in improving various algorithms [32], [33], [34], [35], [36], [37], [38]. The FB technology filtered the training signal within different frequency ranges (i.e., sub-bands), and then trains separate models for the signal in each sub-band. Each sub-band typically has different lower cut-off frequencies and the same upper cut-off frequency (e.g., 90 Hz). During testing, the single-trial test signals are processed using each sub-band model and the sub-band features are computed. The total features are then obtained by linearly combining the sub-band features.

$$\hat{\rho}_k = \sum_{m=1}^{N_b} \alpha(m) \cdot \left(\rho_k^m\right)^2, \alpha(m) = m^{-1.25} + 0.25 \tag{7}$$

where m is the index of filter subbands, N_b is the number of subbands, and ρ_k^m denotes the subband discriminant. Please refer to [7] for details about the weights $\alpha(m)$ and the filtering bandwidth.

3) **Ensemble learning technology**

Ensemble learning technology generally enhances feature recognition efficiency by expanding the dimensions of data or comprehensively utilizing multidimensional information. Nakanishi et al. [6] proposed the ensemble-TRCA (eTRCA) algorithm based on the common-shared spatial filters of low-frequency SSVEP signals. This property was further confirmed in a study by Wong et al. in 2020 [39] that the energy distribution of stimulus-evoked SSVEP signals over a certain frequency range is essentially the same across the scalp. Therefore, the information obtained from covariance matrices corresponding to the signal evoked by other stimuli can also contribute to the training of the target stimulus model. eTRCA enhances the spatial dimensional information of the data by integrating multiple classes of exclusive spatial filters, ultimately performing high-dimensional template matching based on the two-dimensional Pearson correlation coefficient as:

$$\begin{aligned}&\widehat{\boldsymbol{W}} = \left[\widehat{\boldsymbol{\omega}}_1{}^T, \widehat{\boldsymbol{\omega}}_2{}^T, \ldots, \widehat{\boldsymbol{\omega}}_{N_e}{}^T\right]^T \in \mathbb{R}^{N_e \times N_c}, \\ &\rho_k = \operatorname{corr}\left(\widehat{\boldsymbol{W}} \overline{\boldsymbol{X}}_k, \widehat{\boldsymbol{W}} \boldsymbol{Y}\right) \end{aligned} \tag{8}$$

F. Performance Evaluation

1) **Amplitude and Signal to Noise Ratio (SNR) of SSVEPs**

EEG signals from nine occipital electrodes, namely Pz, PO5, PO3, POZ, PO4, PO6, Oz, O1, O2, were selected. Fast Fourier Transform (FFT) was applied to compute the amplitude at the corresponding target frequency. SNR in decibels (dB) was defined as the ratio of $y(f)$ to the value of the 20 neighboring frequencies, 0.24 refers to the shortest distance between two spectral lines in the spectrum diagram.

$$\begin{aligned}&\text{SNR} \\ &= 20 \log_{10} \frac{\mathrm{y}(f)}{\sum_{\mathrm{k}=1}^{10} [\mathrm{y}(f - 0.24 \times k) + \mathrm{y}(f + 0.24 \times k)]} \end{aligned} \tag{9}$$

2) **ITR of SSVEP-BCI** Researchers often use ITR as a comprehensive index to evaluate the performance of a BCI system. ITR was originally used to measure the communication and calculation rate of the system in the field of communication, and was introduced into the field of BCI by Wolpaw et al. [40]. the specific calculation formula is

$$ITR = \frac{60}{T}\left[\log_2 N + p\log_2 p + (1-p)\log_2\left(\frac{1-p}{N-1}\right)\right] \quad (10)$$

where N represents the number of targets, p is the average classification accuracy of all targets, and T is the target selection time, which refers to the total time including eye shift time, the delay of the human visual pathway and the actual duration of the stimulus, which amounted to 1.9 s. The number of targets (i.e., N) was 8 in this study.

G. Statistical Analyses

Statistical analyses were performed using SPSS software (IBM SPSS Statistics, IBM). Two-way repeated-measures analysis of variance (ANOVA) was used to test the interactive effect of presentation forms and distribution pattern on SSVEP classification accuracy and subjective fatigue score in experiment1. Paired t-tests were used to explore whether there were significant differences in amplitude, SNR, classification accuracy and subjective fatigue score between 100%-pixel density and other lower pixel densities in experiment2 and 3, with an alpha level set at 0.05.

III. Result

A. Square-Random Stimulus-Presenting Mode Was More Suitable for Low-Pixel SSVEP

One of the main objectives of experiment 1 was to explore the most suitable stimulus presentation form (flickering square vs. flickering checkerboard) and pixel distribution pattern (random vs. uniform) for low-pixel-density SSVEP. The level of comfort was first studied by measuring the fatigue score. As shown in Fig. 3 (a), in square-random (S-R), square-uniform (S-U), checkerboard-random (C-R), and checkerboard-uniform (C-U) conditions, the fatigue score decreased with the reduction of pixel density. Paired comparisons between any two pixel densities under each condition were listed in TABLE II (left), which preliminarily verified the feasibility of low pixel density in improving user comfort. The interactive effect between presentation form and distribution pattern was then tested under each pixel density. As shown in TABLE I (upper), the checkerboard presentation form achieved a smaller fatigue score than the square presentation form, and the random distribution pattern exhibited a lower fatigue score than the uniform distribution under some pixel-density conditions.

This study further compared the SSVEP classification accuracy calculated by TRCA, a typical SSVEP decoding method. As shown in Fig. 3(b) and TABLE I (lower), the accuracy of flickering square form was approximately 30% higher than

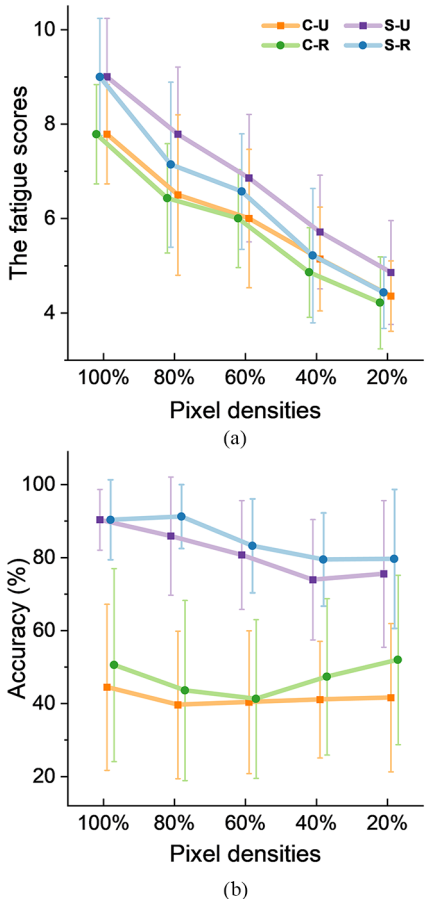

Fig. 3. Average subjective fatigue scores (a) and Average classification accuracy based on the TRCA algorithm (b). Square-uniform, square-random, checkerboard-uniform, and checkerboard-random are S-U, S-R, C-U, and C-R, respectively. Error bars indicate standard deviations (SD).

TABLE I
THE INTERACTIVE EFFECT BETWEEN PRESENTATION FORM AND DISTRIBUTION PATTERN

	Pixel density	Presentation form	Distribution pattern	Presentation form* Distribution pattern
Subjective fatigue scores	100%	**0.000**	1.000	1.000
	80%	**0.001**	**0.003**	0.120
	60%	**0.004**	0.263	0.336
	40%	**0.037**	**0.003**	0.620
	20%	0.078	0.072	0.391
Classification accuracy	100%	**0.000**	1.000	1.000
	80%	**0.000**	0.100	0.781
	60%	**0.000**	0.408	0.800
	40%	**0.000**	**0.042**	0.912
	20%	**0.000**	0.164	0.453

Alpha level was set at 0.05.

that of checkerboard under all the pixel densities (p <0.001). The random distribution pattern had higher accuracy than the uniform distribution, but the difference was significant only at 40%-pixel density ($p = 0.042$). Taking both comfort and effectiveness into account, we found that random pixel distribution achieved a lower fatigue score and higher accuracy than the uniform distribution, while the flickering square had a slightly higher fatigue score but much higher accuracy than the

TABLE II
THE SIGNIFICANT DIFFERENCES AMONG DISTINCT PIXEL DENSITIES UNDER S-U, S-R, C-U, C-R CONDITIONS

	Subjective Fatigue Rating				Classification Accuracy			
Condition	**S-U**	**S-R**	**C-U**	**C-R**	**S-U**	**S-R**	**C-U**	**C-R**
100% vs 80%	**0.000**	**0.000**	**0.005**	**0.000**	0.153	0.817	0.306	0.136
100% vs 60%	**0.000**	**0.000**	**0.000**	**0.000**	**0.017**	0.117	0.449	0.112
100% vs 40%	**0.000**	**0.000**	**0.000**	**0.000**	**0.001**	**0.012**	0.522	0.648
100% vs 20%	**0.000**	**0.000**	**0.000**	**0.000**	**0.025**	0.081	0.625	0.817
80% vs 60%	**0.017**	**0.120**	**0.047**	**0.028**	0.146	**0.013**	0.715	0.614
80% vs 40%	**0.000**	**0.000**	**0.001**	**0.000**	**0.005**	**0.002**	0.562	0.536
80% vs 20%	**0.000**	**0.000**	**0.001**	**0.000**	0.079	**0.033**	0.686	0.120
60% vs 40%	**0.000**	**0.000**	**0.001**	**0.000**	0.095	0.295	0.782	0.125
60% vs 20%	**0.000**	**0.000**	**0.002**	**0.000**	0.239	0.460	0.817	**0.042**
40% vs 20%	**0.005**	0.051	**0.021**	**0.022**	0.774	0.962	0.920	0.395

Alpha level was set at 0.05.

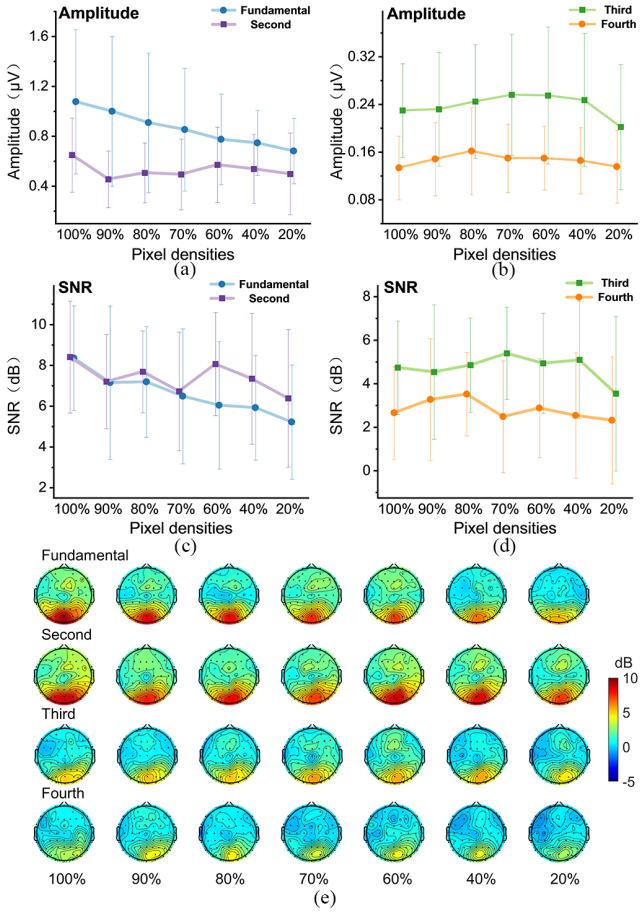

Fig. 4. The amplitude and SNR of SSVEP in experiment 2. (a) Average amplitude at the fundamental and second harmonics, (b) the third and fourth harmonics of SSVEP. (c) Average SNR at the fundamental and second, (d) the third and fourth harmonics of SSVEP. The error bars indicate SD. (e) SNR topographies under distinct pixel densities.

checkerboard form. Thus, the flickering square with random pixel distribution (S-R) was identified as a more suitable stimulus-presenting mode for low-pixel-density SSVEP.

Strikingly, in the S-R condition, the classification accuracy initially increased, reaching its peak at 80%-pixel density with an accuracy of 91.25±8.75%, and then decreased as the pixel density was further reduced. However, due to the multitude of factors involved in experiment 1 (such as presentation form, distribution pattern, pixel density, etc.), it was challenging to thoroughly investigate the influences of pixel densities with smaller percentage intervals. Moreover, experiment 1 required a considerable amount of time to complete which might have an impact on the subjects' performance. To gain a more comprehensive understanding of low-pixel-density SSVEP, another experiment was conducted.

TABLE III
PAIRED T RESULTS BETWEEN DIFFERENT PIXEL DENSITIES FOR EXPERIMENT 2

	Amplitude				SNR			
	Found-amental	Second	Third	Fourth	Found-amental	Second	Third	Fourth
100% - 90%	0.547	**0.000**	0.921	0.156	0.074	**0.049**	0.791	0.394
100% - 80%	0.211	**0.009**	0.464	**0.016**	0.095	0.256	0.840	0.090
100% - 70%	0.070	**0.025**	0.167	**0.024**	**0.020**	**0.028**	0.308	0.763
100% - 60%	**0.009**	0.260	0.255	0.057	**0.006**	0.591	0.776	0.706
100% - 40%	**0.017**	0.115	0.412	0.162	**0.009**	0.202	0.549	0.850
100% - 20%	**0.009**	0.038	0.194	0.867	**0.002**	**0.030**	0.08	0.621

Alpha level was set at 0.05.

B. 60%-90% Is the Ideal Range for Low-Pixel-Density SSVEP

Experiment 2 included seven densities (100%, 90%, 80%, 70%, 60%, 40%, 20%), with each condition having an increased number of trials (i.e., 10) compared to experiment 1.

The amplitudes at the fundamental, second, third, and fourth harmonics of the target frequency were analyzed. As shown in Fig. 4(a), there is a decreasing trend as the pixel density decreases at fundamental frequency. Evident amplitude reductions were found at 60%-, 40%-, and 20%-pixel densities compared to that of 100%, with corresponding p values listed in TABLE III (left). However, as Fig. 4(a) and (b) showed, at the harmonics of target frequency, the amplitudes first decreased and then increased. In particular, the amplitudes at 60%-pixel density (second: 0.57±0.30 μV; third: 0.25±0.11 μV; fourth: 0.15±0.05 μV) were almost the same as those at 100% (second: 0.65±0.29 μV; third: 0.23±0.08 μV; fourth:

0.13±0.05 μV) (significant difference, second: $p = 0.260$; third: $p = 0.255$; fourth: $p = 0.057$). Furthermore, in SNR analyses, as Fig. 4(c) and (d) showed, we found that at 60%-pixel density, the SNR of the second harmonic frequency (8.06±2.53 dB) was almost the same as that of 100%-pixel density (8.41±2.74 dB). Moreover, it was even similar as the SNR of the fundamental frequency (8.35±2.57 dB). The SNR significant differences between any two pixel-densities in the fundamental, second, third, fourth harmonics of the frequency condition are listed in TABLE III (right). SNR topographies depicted in Fig. 4 (e) showed that SNR enhancement primarily occurred in occipital brain area, which is a typical area responding to visual stimuli. Evidently, at both fundamental and harmonics frequencies, stimuli with 60%- to 90%-pixel density exhibited very similar or even higher SNR topographies compared to those of 100%-pixel density. On the other hand, when pixel density is below 60%, SNRs significantly decreased. Amplitude and SNR analyses indicate that the range of 60% to 90% is potentially more suitable range for low-pixel-density SSVEP.

In this study, both the fatigue score and classification accuracy were analyzed, as depicted in Fig. 5. As pixel density decreased, the fatigue score showed a significant decrease, whereas the classification accuracy remained relatively constant until the pixel density dropped below 60%. Specifically, the conventional pixel density (100%) had a significantly higher fatigue score compared to all the low pixel densities (100% vs. 90%: $p = 0.002$; other paired comparisons: $p < 0.001$). Regarding classification accuracy, the values were as follows for different pixel densities: 94.13±7.39%, 93.38±11.20%, 91.93±10.22%, 91.31±9.75%, 91.06±10.17%, 87.56±14.53%, 86.68±11.50% for the pixel density of 100%, 90%, 80%, 70%, 60%, 40%, 20%, respectively. Notably, in the range of 60% to 90% low-pixel density, there was no significant difference in accuracy compared to the 100%-pixel density. However, the accuracies of 40%- and 20%-pixel density were significantly lower than that of 100% (40% vs. 100%: $p = 0.022$; 20% vs. 100%: $p = 0.009$). Moreover, subjects with poor classification accuracy showed a more obvious decline at 40%- and 20%- pixel density, and the overall trend was still in line with the average results. These results further verify the feasibility of using 60%- to 90%-pixel density stimuli to optimize SSVEP-BCI. Therefore, a 60%-pixel density SSVEP achieved both lower fatigue scores and a high classification accuracy, making it a promising choice for SSVEP-BCI applications.

The above classification accuracy was obtained by using the TRCA method. As recent advances in algorithmic methods have enhanced the decoding performance for weak stimuli, this study also used improved TRCA algorithms (FB-TRCA, eTRCA, FB-eTRCA) to decode the responses induced by low-pixel-density SSVEP. An interesting finding is that the advanced algorithms show improved decoding performance under lower pixel density conditions. Specifically, for 100%-pixel density, there is little difference among the four algorithms, which were 94.13±7.39%, 95.06±6.22%, 94.05±7.53% and 94.31±7.13%, respectively. When the pixel density decreases to 80% or less, a noticeable trend in accuracy

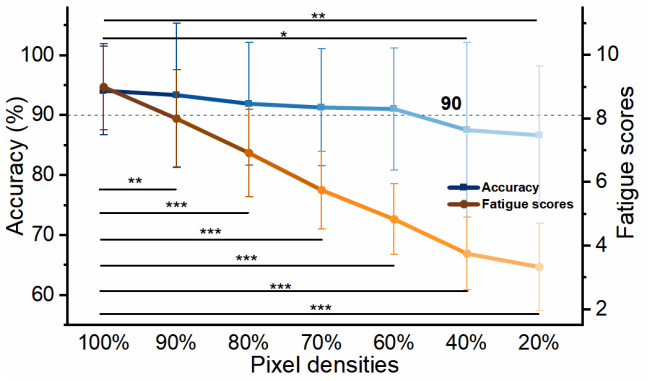

Fig. 5. Average classification accuracy based on TRCA under square-random stimulus-presenting mode and average subjective fatigue scores of 20 subjects in experiment 2. Error bars indicate SD. Asterisks indicate a significant difference between each pair by paired samples t-test (*$p < 0.05$, **$p < 0.01$, ***$p < 0.001$).

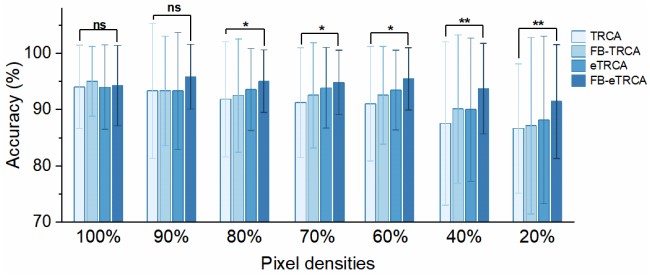

Fig. 6. Performance of four classification algorithms (TRCA, FB-TRCA, eTRCA, FB-eTRCA) under different pixel densities in experiment 2. Error bars indicate SD. Asterisks indicate a significant difference between each pair by paired samples t-test (*$p < 0.05$, **$p < 0.01$, ***$p < 0.001$).

emerges, with TRCA<FB-TRCA<eTRCA<FB-eTRCA. This trend indicates that FB-eTRCA can achieved better decoding accuracy. At 60%-pixel density, the accuracies of TRCA and its advanced algorithms were 91.06±10.17%, 93.94±6.39%, 94.25±6.40% and 95.50±5.55%, respectively. The accuracy of FB-TRCA, eTRCA, FB-eTRCA was 2.87%, 3.19%, 4.44% higher than that of TRCA (TRCA vs. FB-TRCA: $p = 0.044$, TRCA vs. eTRCA: $p = 0.023$, TRCA vs. FB-eTRCA: $p = 0.015$). At 40%-pixel density, FB-TRCA, eTRCA, FB-eTRCA was 4.56%, 3.75%, 6.25% higher than the TRCA (TRCA vs. FB-TRCA: $p = 0.004$, TRCA vs. eTRCA: $p = 0.002$, TRCA vs. FB-eTRCA: $p = 0.003$). Similarly, at 20%-pixel density, the corresponding improved accuracies were 3.06%, 3.44%, and 4.81% (TRCA vs. FB-TRCA: $p = 0.027$, TRCA vs. eTRCA: $p = 0.004$, TRCA vs. FB-eTRCA: $p = 0.004$). These results indicate that the classification accuracy can be further improved by using more effective decoding methods.

C. SSVEP With 60%-Pixel Density Achieved Satisfactory Performance in Online Test

According to the above results, this study selected a square-random presentation pattern with distinct pixel densities (100%, 80%, 60%, 40%, 20%) for the online test, and FB-eTRCA was used as the decoding method. As shown in Fig. 7, the fatigue scores were 8.75±1.37, 6.58±1.83, 5.58±1.62, 4.08±1.67, and 3.25±2.18, indicating a decrease in fatigue as the pixel density reduced (100% vs. 80%: $p < 0.01$; 100% vs. 60%: $p < 0.001$; 100% vs.

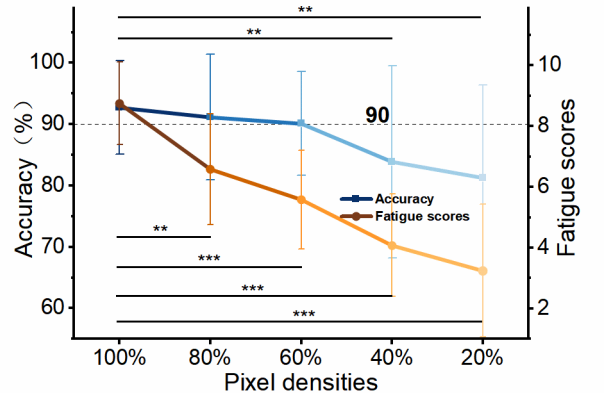

Fig. 7. Average accuracy and fatigue score of 12 subjects in online experiment. Error bars indicate SD. Asterisks indicate a significant difference between each pair by paired samples t-test (*$p < 0.05$, **$p < 0.01$, ***$p < 0.001$).

40%: $p < 0.001$; 100% vs. 20%: $p < 0.001$). The online accuracy was 92.71±7.63%, 91.15±10.26%, 90.10±8.44%, 83.85±15.62%, and 81.25±15.14% for 100%-, 80%-, 60%, 40%, 20%-pixel-density SSVEP, respectively. There was no significant difference between 60%-, 80%- and 100%-pixel density (100% vs. 80%: $p = 0.167$, 100% vs. 60%: $p = 0.148$), but accuracy of 40%- and 20%-pixel density decreased significantly (100% vs. 40%: $p = 0.004$; 100% vs. 20%: $p = 0.003$). The ITR was also calculated and compared, resulting in values of 78.37±15.45 bits/min, 76.02±18.88 bits/min, 73.12±16.11 bits/min, 64.26±24.61 bits/min, 59.48±22.96 bits/min, respectively. The ITR statistical analysis between any two pixel-densities showed similar trends to the accuracy results. Therefore, the online test verified that the SSVEP with 60%-pixel density can significantly improve comfort while maintaining effectiveness, making it an appropriate pixel density choice.

IV. Discussion

The current study aimed to achieve a perfect balance between comfort and effectiveness of SSVEP-BCI by reducing the pixel density of stimuli. We found that stimuli with 60%-pixel density and a square-uniform presentation-distribution mode achieved significantly better comfort scores while maintaining almost the same classification accuracy as that of 100%-pixel density in both the offline and online tests. These results confirmed the feasibility of improving the comfort of SSVEP by using stimuli with 60%-pixel density, providing new insights for optimizing SSVEP-BCI.

One novel aspect of this study is the manipulation of pixel density. It's essential to differentiate pixel density from contrast, as they are two distinct concepts. Contrast refers to the difference between the highest and lowest grayscale values in an image [14]. It is a physical quantity related to optical systems and can be expressed in terms of maximum brightness difference, reflecting the ability to resolve between light and dark areas in an image [13], [15]. On the other hand, pixel density refers to the proportion of luminous pixels within each unit area of the image, reflecting the richness of detailed information in an image. Lowering pixel density reduces the number of luminous pixels without altering the brightness settings or the contrast of the stimuli. Interestingly, reducing pixel density increases the number of boundaries between light and dark areas in the stimuli, potentially contributing to enhanced neural responses, as discussed in introduction section. One study [41] designed ON and OFF grid stimulation paradigms based on the ON-OFF cell conduction pathway to explore the effect of contrast, and designed to remove weak stimuli by reducing the relative light intensity of the flickering region to the background grid, but this is fundamentally different from our study. In our experiment, the variable was pixel density, whereas the contrast was always the same.

Stimuli with low-pixel density improved SSVEP comfort by decreasing overall intensity. In the traditional view, it might lead to decreased neural responses, negatively impacting the BCI effectiveness. However, this study observed no significant amplitude, SNR or classification accuracy difference between 100%- and other low-pixel densities (90%-, 80%-, 70%-, 60%-pixel density). This novel observation confirms that the boundary-related enhancement caused by the center-periphery antagonism effect indeed works in the SSVEP paradigm, benefiting comfort without compromising effectiveness. Furthermore, this study identified 60% as the most suitable pixel density for achieving the ideal balance between comfort and effectiveness. This result could potentially be explained by the differences in boundary length between light and dark pixels within a stimulus. In our simulation calculations, the boundaries within a single stimulus were calculated under distinct pixel density conditions, results revealed the total length of boundary first increases and then decreases with the reduction of pixel density, peaking in the range of 40%-∼60%-pixel density. This indicates that within the range of 100% to 60%-pixel density, the stimulus intensity decreases, but there is an increase in the total length of light-dark boundaries, counteracting the reduced neural responses caused by intensity reduction. However, when stimulus intensity is less than 60%, the length of the light-dark boundary also decreases, making it difficult to resist the intensity-related decreases, leading to an overall decrease in the SSVEP response.

There might be another factor contributing to why the 60%-pixel density balanced the comfort and effectiveness of SSVEP-BCI. In the typical SSVEP paradigm, subjects need to focus on the target stimulus while ignoring other stimuli that simultaneously flicker at different frequencies. The center-periphery antagonistic effect of the retina discussed above mainly works to process the target stimulus when sufficient attentional resources are allocated to it. However, this effect may not be as effective in dealing with other non-target stimuli [42], leading to neural responses induced by non-target stimuli mainly relying on the stimulus intensity. Consequently, from an overall stimulation interface perspective, as pixel density decreases, the intensity of all stimuli is reduced, while the retinal response to the target stimulus remains largely unchanged, and responses induced by other non-target stimuli decrease. According to the definition of SNR, the target frequency is regarded as the signal, which remains unchanged, while other frequencies are regarded as noise, which decreases with the reduction in pixel density. This reduction in pixel density effectively improves the

signal-to-noise ratio, as supported by the SNR results shown in Fig. 4. This study revealed that the presentation form (square vs. checkerboard) had an impact on the performance of low-pixel-density SSVEP-BCI, where the classification accuracy of checkerboard was significantly lower than that of flickering square. This observation may be attributed to the different spatial frequencies and stimuli phases. To be specific, previous findings by Ming et al. [43] and Waytowich et al. [44] indicated that the SSVEP accuracy fluctuated as the spatial frequency of checkerboard increased; in particular, the accuracy decreased from 0 (i.e., square) to about 0.3 cycle/° spatial frequency. The 3×3 checkerboard used in this study had a spatial frequency of 0.263 cycle/°, explaining the lower accuracy of checkerboard compared to square, and consistent with these findings. Moreover, the lower accuracy of checkerboard might also be explained by phase inversion. Previous studies have demonstrated that SSVEP response is a superimposed response of the primary visual cortex to several stimuli received at the same time [45]. Here, in the checkerboard paradigm, a small grid of a checkerboard (there were nine grids in a checkerboard) was surrounded by other grids that had a phase difference of π from its initial phase. This implies that the neural response induced by a checkerboard essentially contains two kinds of responses: one induced by the grids with an initial phase of 0, and others induced by the grids with π phase. These two responses with opposite phases may cancel each other out, leading to a smaller response than that induced by a square.

This study also found that the random distribution pattern achieved better SSVEP performance and higher comfort scores than uniform patterns. This observation may be explained by the difference in the angle of view between the two patterns. The angle of view can be calculated as follows:

$$\beta = 2arctan(\frac{D}{2 * L}) \tag{11}$$

where D is the side length of the stimulation, L is the distance between the subject's eyes and the display, which is fixed at 50cm in the experiment. A 24-inch monitor was used, which was 53.15 cm in length and 29.90 cm in width, and the resolution was 1920∗1080. Thus, the side length of a single pixel was 0.276852mm, the corresponding angle of view was about 0.03°. As we all known, the least angle of view that human beings can constrainedly discriminate is 0.017°, 0.03° is already a very small angle of view that is not easy enough for subjects to clearly discriminate the boundaries between dark and light [46], which resulted in a reduction of boundaries that can be perceived by subjects. If so, the increased boundaries caused by low-pixel density would not work effectively to induce larger neural responses. However, in random distribution pattern, some pixels gathered to make up a part of stimuli, the corresponding angle of view usually much larger than 0.03°, making boundaries easier to discriminate. The boundaries that easier for discrimination could account for the higher comfort and accuracy related to random distribution pattern.

This study provides valuable insights for future research in two aspects. First, as decoding algorithms advance, the pixel density required to perfectly balance the comfort and effectiveness of SSVEP can be lower. In this study, we compared the decoding performance of TRCA, which is the most classical for SSVEP decoding, and another three improved methods, including FB-TRCA, eTRCA and FB-eTRCA. On one hand, the introduction of FB-technology can improve classification performance, especially at low pixel density. As pixel density reduces, TRCA performance decreases due to the energy reduction of the fundamental frequency, and the SD between subjects also increases (100%-20%: SD=7.39%, 11.96%, 10.22%, 9.75%, 10.17%, 14.53%, 11.50%). The introduction of FB-technology enables better utilization of SSVEP harmonic information, resulting in higher accuracies at low-pixel densities. On the other hand, the introduction of ensemble learning enhances the stability of the algorithm and the utilization rate of different types of data information, demonstrating superior decoding accuracy. These results further indicated the urgent need for a more advanced decoding algorithm capable of extracting useful information from very weak or small SSVEP responses. Second, while this study focused on neural responses and decoding accuracy under low-pixel-density and low-frequency conditions, the feasibility of low-pixel-density SSVEP-BCI remains unknown at higher stimulation frequency. Combining the advantages of both low-pixel-density and high-frequency SSVEP could lead to more advanced SSVEP-BCI with higher ITR and lower fatigue.

V. Conclusion

This study proposed a novel low-pixel-density encoding paradigm to improve the comfort of SSVEP-BCI while maintaining system effectiveness. The flickering square with a random pixel distribution proved to be a more suitable presentation pattern of stimuli, and 60% was identified as the optimal pixel density for achieving the perfect balance between comfort and effectiveness. These results contribute to the advancement of more natural BCI.

References

[1] J. R. Wolpaw et al., "Brain–computer interface technology: A review of the first international meeting," *IEEE Trans. Rehabil. Eng.*, vol. 8, no. 2, pp. 164–173, Jun. 2000.

[2] A. Kawala-Sterniuk et al., "Summary of over fifty years with brain–computer interfaces—A review," *Brain Sci.*, vol. 11, no. 1, p. 43, Jan. 2021.

[3] Y. Wang, M. Nakanishi, and D. Zhang, "EEG-based brain–computer interfaces," in *Neural Interface: Frontiers and Applications* (Advances in Experimental Medicine and Biology), vol. 1101. Cham, Switzerland: Springer, Nov. 2019, pp. 41–65.

[4] J. Tang et al., "Optimizing SSVEP-based BCI system towards practical high-speed spelling," *Sensors*, vol. 20, no. 15, p. 4186, Jul. 2020.

[5] R. Zerafa, T. Camilleri, O. Falzon, and K. P. Camilleri, "To train or not to train? A survey on training of feature extraction methods for SSVEP-based BCIs," *J. Neural Eng.*, vol. 15, no. 5, Oct. 2018, Art. no. 051001.

[6] M. Nakanishi, Y. Wang, X. Chen, Y.-T. Wang, X. Gao, and T.-P. Jung, "Enhancing detection of SSVEPs for a high-speed brain speller using task-related component analysis," *IEEE Trans. Biomed. Eng.*, vol. 65, no. 1, pp. 104–112, Jan. 2018.

[7] X. Chen, Y. Wang, S. Gao, T.-P. Jung, and X. Gao, "Filter bank canonical correlation analysis for implementing a high-speed SSVEP-based brain–computer interface," *J. Neural Eng.*, vol. 12, no. 4, Aug. 2015, Art. no. 046008.

[8] Z. Lin, C. Zhang, W. Wu, and X. Gao, "Frequency recognition based on canonical correlation analysis for SSVEP-based BCIs," *IEEE Trans. Biomed. Eng.*, vol. 54, no. 6, pp. 1172–1176, Jun. 2007.

[9] X. Chen, Y. Wang, M. Nakanishi, X. Gao, T.-P. Jung, and S. Gao, "High-speed spelling with a noninvasive brain–computer interface," *Proc. Nat. Acad. Sci. USA*, vol. 112, no. 44, pp. 6058–6067, Nov. 2015.

[10] A. Funase, K. Wakita, A. Itai, and I. Takumi, "SSVEP by checkerboard related to grid size and board size," in *Proc. Asia–Pacific Signal Inf. Process. Assoc. Annu. Summit Conf. (APSIPA)*, Dec. 2015, pp. 1141–1144.

[11] N.-S. Kwak, D.-O. Won, K.-T. Kim, H.-J. Park, and S.-W. Lee, "Analysis of steady state visual evoked potentials based on viewing distance changes for brain–machine interface speller," in *Proc. IEEE Int. Conf. Syst., Man, Cybern. (SMC)*, Oct. 2016, pp. 001502–001505.

[12] Y. Gao, A. Ravi, and N. Jiang, "Does inter-stimulus distance influence the decoding performance of SSVEP and SSMVEP BCI?" in *Proc. 10th Int. IEEE/EMBS Conf. Neural Eng. (NER)*, May 2021, pp. 507–510.

[13] M. Benda and I. Volosyak, "Comparison of different visual feedback methods for SSVEP-based BCIs," *Brain Sci.*, vol. 10, no. 4, p. 240, Apr. 2020.

[14] X. Zheng et al., "Objective and quantitative assessment of visual acuity and contrast sensitivity based on steady-state motion visual evoked potentials using concentric-ring paradigm," *Documenta Ophthalmologica*, vol. 139, no. 2, pp. 123–136, Oct. 2019.

[15] H. Si-Mohammed et al., "On the effect of size and contrast of the SSVEP visual Stimuations on classification accuracy and user-friendliness in virtual reality," in *Proc. 11th Int. Winter Conf. Brain-Comput. Interface (BCI)*, Feb. 2023, pp. 1–6.

[16] X. Duart, E. Quiles, F. Suay, N. Chio, E. García, and F. Morant, "Evaluating the effect of stimuli color and frequency on SSVEP," *Sensors*, vol. 21, no. 1, p. 117, Dec. 2020.

[17] Y.-Y. Chien et al., "Polychromatic SSVEP stimuli with subtle flickering adapted to brain-display interactions," *J. Neural Eng.*, vol. 14, no. 1, Feb. 2017, Art. no. 016018.

[18] M. Xu, F. He, T.-P. Jung, X. Gu, and D. Ming, "Current challenges for the practical application of electroencephalography-based brain–computer interfaces," *Engineering*, vol. 7, no. 12, pp. 1710–1712, Dec. 2021.

[19] M. H. Chang, H. J. Baek, S. M. Lee, and K. S. Park, "An amplitude-modulated visual stimulation for reducing eye fatigue in SSVEP-based brain–computer interfaces," *Clin. Neurophysiol.*, vol. 125, no. 7, pp. 1380–1391, Jul. 2014.

[20] X. Chai, Z. Zhang, K. Guan, T. Zhang, J. Xu, and H. Niu, "Effects of fatigue on steady state motion visual evoked potentials: Optimised stimulus parameters for a zoom motion-based brain–computer interface," *Comput. Methods Programs Biomed.*, vol. 196, Nov. 2020, Art. no. 105650.

[21] M. Li, X. Chen, and H. Cui, "A high-frequency SSVEP-BCI system based on simultaneous modulation of luminance and motion using intermodulation frequencies," *IEEE Trans. Neural Syst. Rehabil. Eng.*, vol. 31, pp. 2603–2611, 2023.

[22] X. Chen et al., "Optimizing stimulus frequency ranges for building a high-rate high frequency SSVEP-BCI," *IEEE Trans. Neural Syst. Rehabil. Eng.*, vol. 31, pp. 1277–1286, 2023.

[23] M. Li et al., "A novel SSVEP brain–computer interface system based on simultaneous modulation of luminance and motion," *IEEE Trans. Neural Syst. Rehabil. Eng.*, vol. 31, pp. 1149–1157, 2023.

[24] S. Ladouce, L. Darmet, J. J. T. Tresols, S. Velut, G. Ferraro, and F. Dehais, "Improving user experience of SSVEP BCI through low amplitude depth and high frequency stimuli design," *Sci. Rep.*, vol. 12, no. 1, p. 8865, May 2022.

[25] H. Li et al., "Asymmetries of dark and bright negative afterimages are paralleled by subcortical ON and OFF poststimulus responses," *J. Neurosci.*, vol. 37, no. 8, pp. 1984–1996, Feb. 2017.

[26] X. Liu et al., "From receptive to perceptive fields: Size-dependent asymmetries in both negative afterimages and subcortical on and off post-stimulus responses," *J. Neurosci.*, vol. 41, no. 37, pp. 7813–7830, Sep. 2021.

[27] E. V. Famiglietti and H. Kolb, "Structural basis for on-and off-center responses in retinal ganglion cells," *Science*, vol. 194, no. 4261, pp. 193–195, Oct. 1976.

[28] G. Zurawel, I. Ayzenshtat, S. Zweig, R. Shapley, and H. Slovin, "A contrast and surface code explains complex responses to black and white stimuli in V1," *J. Neurosci.*, vol. 34, no. 43, pp. 14388–14402, Oct. 2014.

[29] A. M. Norcia, A. Yakovleva, B. Hung, and J. L. Goldberg, "Dynamics of contrast decrement and increment responses in human visual cortex," *Translational Vis. Sci. Technol.*, vol. 9, no. 10, p. 6, Sep. 2020.

[30] H. Tanaka, T. Katura, and H. Sato, "Task-related component analysis for functional neuroimaging and application to near-infrared spectroscopy data," *NeuroImage*, vol. 64, pp. 308–327, Jan. 2013.

[31] H. Tanaka, T. Katura, and H. Sato, "Task-related oxygenation and cerebral blood volume changes estimated from NIRS signals in motor and cognitive tasks," *NeuroImage*, vol. 94, pp. 107–119, Jul. 2014.

[32] Y. Zhang et al., "Correlated component analysis for enhancing the performance of SSVEP-based brain–computer interface," *IEEE Trans. Neural Syst. Rehabil. Eng.*, vol. 26, no. 5, pp. 948–956, May 2018.

[33] Y. Zhang, S. Q. Xie, C. Shi, J. Li, and Z.-Q. Zhang, "Cross-subject transfer learning for boosting recognition performance in SSVEP-based BCIs," *IEEE Trans. Neural Syst. Rehabil. Eng.*, vol. 31, pp. 1574–1583, 2023.

[34] C. M. Wong, Z. Wang, B. Wang, A. Rosa, T.-P. Jung, and F. Wan, "Enhancing detection of multi-frequency-modulated SSVEP using phase difference constrained canonical correlation analysis," *IEEE Trans. Neural Syst. Rehabil. Eng.*, vol. 31, pp. 1343–1352, 2023.

[35] B. Liu, X. Chen, N. Shi, Y. Wang, S. Gao, and X. Gao, "Improving the performance of individually calibrated SSVEP-BCI by task-discriminant component analysis," *IEEE Trans. Neural Syst. Rehabil. Eng.*, vol. 29, pp. 1998–2007, 2021.

[36] C. M. Wong et al., "Inter- and intra-subject transfer reduces calibration effort for high-speed SSVEP-based BCIs," *IEEE Trans. Neural Syst. Rehabil. Eng.*, vol. 28, no. 10, pp. 2123–2135, Oct. 2020.

[37] J. Huang, P. Yang, B. Xiong, B. Wan, K. Su, and Z.-Q. Zhang, "Latency aligning task-related component analysis using wave propagation for enhancing SSVEP-based BCIs," *IEEE Trans. Neural Syst. Rehabil. Eng.*, vol. 30, pp. 851–859, 2022.

[38] Y. Zhang et al., "Two-stage frequency recognition method based on correlated component analysis for SSVEP-based BCI," *IEEE Trans. Neural Syst. Rehabil. Eng.*, vol. 26, no. 7, pp. 1314–1323, Jul. 2018.

[39] C. M. Wong et al., "Learning across multi-stimulus enhances target recognition methods in SSVEP-based BCIs," *J. Neural Eng.*, vol. 17, no. 1, Jan. 2020, Art. no. 016026.

[40] J. R. Wolpaw, N. Birbaumer, D. J. McFarland, G. Pfurtscheller, and T. M. Vaughan, "Brain–computer interfaces for communication and control," *Clin. Neurophysiol.*, vol. 113, no. 6, pp. 767–791, Jun. 2002.

[41] G. Ming, H. Zhong, W. Pei, X. Gao, and Y. Wang, "A new grid stimulus with subtle flicker perception for user-friendly SSVEP-based BCIs," *J. Neural Eng.*, vol. 20, no. 2, Mar. 2023, Art. no. 026010.

[42] J.-M. Hopf, C. N. Boehler, S. J. Luck, J. K. Tsotsos, H.-J. Heinze, and M. A. Schoenfeld, "Direct neurophysiological evidence for spatial suppression surrounding the focus of attention in vision," *Proc. Nat. Acad. Sci. USA*, vol. 103, no. 4, pp. 1053–1058, Jan. 2006.

[43] G. Ming, W. Pei, H. Chen, X. Gao, and Y. Wang, "Optimizing spatial properties of a new checkerboard-like visual stimulus for user-friendly SSVEP-based BCIs," *J. Neural Eng.*, vol. 18, no. 5, Oct. 2021, Art. no. 056046.

[44] N. R. Waytowich, Y. Yamani, and D. J. Krusienski, "Optimization of checkerboard spatial frequencies for steady-state visual evoked potential brain–computer interfaces," *IEEE Trans. Neural Syst. Rehabil. Eng.*, vol. 25, no. 6, pp. 557–565, Jun. 2017.

[45] H.-J. Hwang, D. Hwan Kim, C.-H. Han, and C.-H. Im, "A new dual-frequency stimulation method to increase the number of visual stimuli for multi-class SSVEP-based brain–computer interface (BCI)," *Brain Res.*, vol. 1515, pp. 66–77, Jun. 2013.

[46] D. Betancourt and C. del Rio, "Study of the human eye working principle: An impressive high angular resolution system with simple array detectors," in *Proc. 4th IEEE Workshop Sensor Array Multichannel Process.*, Jul. 2006, pp. 93–97.